Heterogeneous Catalysis Hot Paper

DOI: 10.1002/anie.201306620

How Strain Affects the Reactivity of Surface Metal Oxide Catalysts**

*Kazuhiko Amakawa, Lili Sun, Chunsheng Guo, Michael Hävecker, Pierre Kube, Israel E. Wachs, Soe Lwin, Anatoly I. Frenkel, Anitha Patlolla, Klaus Hermann, Robert Schlögl, and Annette Trunschke**

Abstract: *Highly dispersed molybdenum oxide supported on mesoporous silica SBA-15 has been prepared by anion exchange resulting in a series of catalysts with changing Mo densities (0.2–2.5 Mo atoms nm^{-2}). X-ray absorption, UV/Vis, Raman, and IR spectroscopy indicate that doubly anchored tetrahedral dioxo MoO_4 units are the major surface species at all loadings. Higher reducibility at loadings close to the monolayer measured by temperature-programmed reduction and a steep increase in the catalytic activity observed in metathesis of propene and oxidative dehydrogenation of propane at 8% of Mo loading are attributed to frustration of Mo oxide surface species and lateral interactions. Based on DFT calculations, NEXAFS spectra at the O-K-edge at high Mo loadings are explained by distorted MoO_4 complexes. Limited availability of anchor silanol groups at high loadings forces the MoO_4 groups to form more strained configurations. The occurrence of strain is linked to the increase in reactivity.*

In 1925, Sir H. S. Taylor proposed that special active sites in a non-balanced state (e.g. low-coordinated species), which represent only a fraction of the surface atoms, are responsible for heterogeneous catalysis.[1] It took decades until the concept earned experimental and theoretical confirmation. Surface science demonstrated that low-coordinated atoms at the edge of steps are indeed the most active in metal catalysts.[2] Recent advances in materials characterization revealed that Taylor's concept is also applicable to high-performing, multi-component catalysts, for example, nanostructured Cu/ZnO for methanol synthesis[3] and gold nanoparticles supported on TiO_2,[4] wherein ensemble sites formed at surface defects or at the metal/oxide interface play a crucial role for catalytic behavior.

Monolayer-type supported metal oxides are another important class of heterogeneous catalysts, in which the supported metal oxide phase is present as a two-dimensional surface overlayer. They also show differences in the reactivity of the individual surface metal oxide species. For example, only approximately 1.5% of the molybdenum atoms are active in olefin metathesis on silica-supported molybdenum oxide catalysts, a situation in line with Taylor's concept.[5] The catalytic performance of supported metal oxides sometimes shows a non-linear dependence on the metal oxide loading where the activity develops steeply above a certain level of surface coverage.[6–10] Reasons for this general observation, however, remain elusive.

Herein, silica-supported molybdenum oxides, which represent models for oxidation[8] and metathesis[5,9] catalysts, were chosen to exemplify the impact of surface metal oxide coverage on reactivity. Dehydrated[11] molybdenum oxide supported on mesoporous silica SBA-15 (MoO_x/SBA-15) was initially studied by temperature-programmed reduction with hydrogen (H_2-TPR) as a test reaction.[6,9,10] The H_2-TPR profiles (Figure 1) reveal enhanced reducibility with increasing Mo oxide loading. At the lowest loading (2.1% Mo), a single, sharp reduction peak is observed at 1158 K. Upon increasing the Mo oxide loading, in addition to the progressive broadening of the high-temperature peak, a new distinct low-temperature peak at 856 K occurs, indicating the cumulative appearance of surface molybdenum oxide species that have a higher reducibility.

The effect of surface coverage on the reactivity of monolayer transition-metal oxides has been attributed to changes in the degree of polymerization, for example, the appearance of monomeric, polymeric, and nano-crystalline domains.[7] However, spectroscopy reveals only modest structural modifications with increasing surface coverage. The very similar fingerprints in UV/Vis spectroscopy and the Mo K-edge of the X-ray absorption near-edge structure (XANES;

[*] Dr. K. Amakawa, Dr. L. Sun, Dr. C. Guo, Dr. M. Hävecker, P. Kube, Prof. Dr. K. Hermann, Prof. Dr. R. Schlögl, Dr. A. Trunschke
Department of Inorganic Chemistry
Fritz-Haber-Institut der Max-Planck-Gesellschaft
Faradayweg 4-6, 14195 Berlin (Deutschland)
E-mail: trunschke@fhi-berlin.mpg.de
Homepage: http://www.fhi-berlin.mpg.de/
Dr. M. Hävecker
Department of Solar Energy Research
Helmholtz-Zentrum Berlin/BESSY II
Albert-Einstein-Strasse 15, 12489 Berlin (Deutschland)
Prof. Dr. I. E. Wachs, S. Lwin
Operando Molecular Spectroscopy & Catalysis Laboratory
Department of Chemical Engineering, Lehigh University
Bethlehem, Pennsylvania 18015 (USA)
Prof. Dr. A. I. Frenkel, Dr. A. Patlolla
Department of Physics, Yeshiva University
245 Lexington Avenue, New York, NY 10016 (USA)

[**] We thank G. Weinberg, Dr. T. Cotter, M. Hashagen, G. Lorenz, Dr. F. Girgsdies, E. Kitzelmann, A. Klein-Hoffmann, C. V. T. Nguyen, the NSLS staff, and the HZB staff for their professional assistance. I.E.W. thanks the Alexander von Humboldt Foundation (Germany), for the Humboldt Research Award. A.I.F. acknowledges the U.S. DOE Grant No. DE-FG02-05ER15688 for supporting X18B beamline operations. S.L. acknowledges financial support from U.S. DOE-Basic Energy Sciences (Grant No. FG02-93ER14350). K.A. is grateful to Mitsubishi Gas Chemical Co. Inc. for a fellowship.

Supporting information for this article is available on the WWW under http://dx.doi.org/10.1002/anie.201306620.

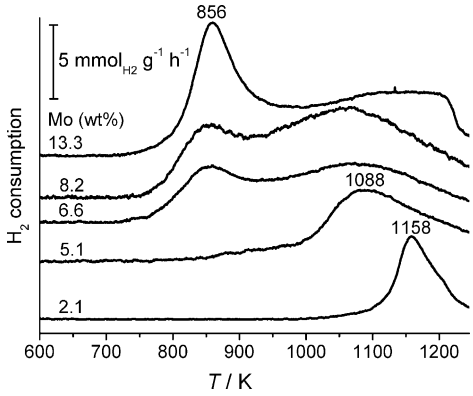

Figure 1. Temperature-programmed reduction (H_2-TPR) of supported MoO_x/SBA-15 measured at a heating rate of 10 K min^{-1} in 2% H_2 in Ar after pretreatment in 20% O_2 in Ar at 823 K for 0.5 h.

Figure 2a,b) indicate little change in the connectivity of surface molybdenum oxide[12] or in the coordination geometry. The molybdenum has a predominantly tetrahedral coordination, similar to the reference compound $Al_2(MoO_4)_3$, as suggested by the intense pre-edge peak at 20006 eV (Figure 2b). Fourier-transformed Mo K-edge extended X-ray absorption fine structure (EXAFS) spectra (Figure 2c) show

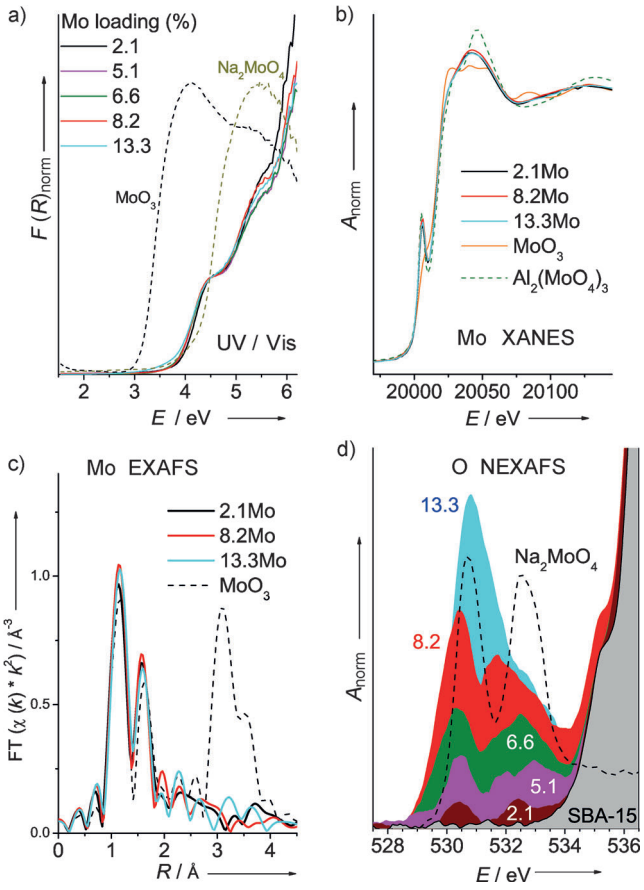

Figure 2. a) UV/Vis, b) Mo K-edge XANES, c) Fourier-transformed phase-uncorrected Mo K-edge EXAFS, and d) O K-edge NEXAFS spectra of dehydrated MoO_x/SBA-15.

two distinct distances at $R < 2$ Å, which are assigned to Mo=O double and Mo–O single bonds based on the observed vibrational bands in the Raman/IR analysis[13–16] (Supporting Information; Figure S6, 980–997 cm^{-1} for Mo=O, and 926–943 cm^{-1} for Mo–O). Conclusive structural assignment is provided by near-edge X-ray absorption fine structure (NEXAFS) analysis at the oxygen K-edge combined with DFT calculations. The double-peak absorption at the O 1s edge (Figure 2d; peaks at 530.2 and 532.5 eV) observed at low loadings is well reproduced by DFT calculations[17] considering models having doubly anchored di-oxo (Si-O-)$_2$Mo(=O)$_2$ structures characterized by an Si–Si distance of 4.6–4.7 Å (clusters **a** and **b** in Figure S1, Figure S5A, Table S1). In accordance with this result, the fitting of the first coordination sphere of Mo in the K-edge EXAFS using a di-oxo (O-)$_2$Mo(=O)$_2$ model reproduces the experimental spectra well, yielding Mo–O path lengths consistent with the theoretical prediction (Figure S1, S4, Tables S1, S3). Moreover, the calculated IR spectra of the di-oxo models are in agreement with the experimental IR spectra (Figure S6D, S7). All the results indicate that the doubly anchored tetrahedral di-oxo (Si-O-)$_2$Mo(=O)$_2$ unit represents the major surface molybdenum oxide species, which is also in agreement with previous reports.[13–17]

While the bond lengths obtained by EXAFS fitting are independent of the Mo loading (Table S3), subtle structural variations are clearly imprinted in the O K-edge NEXAFS data. With increasing loading the O K-edge NEXAFS feature arising from the molybdenum oxide (528–534 eV) gradually loses its well-separated double peak structure as the peaks broaden and a new component emerges at 531 eV (Figure 2d). The peak broadening and the occurrence of the new peak seem to be linked to the changes in the H_2-TPR profiles (Figure 1; broadening of the high-temperature peak and the occurrence of the low-temperature peak at 856 K). The broad NEXAFS feature is in clear contrast to the well-separated double peak corresponding to crystalline Na_2MoO_4 (Figure 2d) that consists of uniform isolated MoO_4 units. This difference implies changes in the bond angles as a result of variations in the Mo–Si distance with increasing loading. The Fourier transform of the Mo K-edge EXAFS at longer R (Figure 2c) shows neither distinct peaks nor systematic changes upon increasing the Mo loading, which indicates the absence of a well-defined geometrical order beyond the first coordination sphere and suggests, in turn, a broad distribution of the Mo–Si distances in the anchoring Mo-O-Si motifs. The various Mo–Si distances originate from the amorphous nature of the silica surface. On the surface there is a wide range of Si–Si distances between the silanol pairs used for anchoring of the di-oxo structures.[13,18,19] This leads to variations in the Mo-O-Si angle and the O–Si length. In addition, four-coordinate pentahedral mono-oxo (Si-O-)$_4$-Mo=O structures may occur as a minority species when four silanol sites are suitably arranged.[13] In fact, we observe additional vibrational bands assigned to the mono-oxo species[13,14] in the resonance Raman spectrum. The resonance Raman technique detects minority species that are invisible in non-resonant Raman spectroscopy (Figure S8).

Surface silanol groups are consumed by forming Mo–O–Si bridging bonds. The density of isolated silanol sites drops from 1.6 (bare SBA-15) to 0.07 (13.3 % Mo) sites per square nanometer (Table S2, Figure S6 C), revealing a highly "silanol deficient" state at high Mo oxide surface coverage. Given the limited availability of silanol OH groups at high coverage, the formation of surface Mo oxide species having more than one anchoring bond (e.g. doubly anchored di-oxo structures) increases the structural strain. The models in Figure 3 illustrate the idea schematically. The two-dimensional (*x*–*y* axes) description in Figure 3 a shows a network of siloxane rings of various ring sizes,[18,20] while another two-dimensional description in Figure 3 b reminds us that in real 3D space there is also a variation along the *z* axis. In Figure 3 a, the di-oxo MoO_4 units are anchored on less-strained configurations at low molybdenum coverage, whereas the decrease in the number of silanol sites forces the di-oxo MoO_4 structures to form more strained configurations. The distribution of species is governed by their thermodynamic stability[21] due to the high surface mobility of the Mo oxide.[11,22] In the 2D description, the geometric constraint may be approximated by the size of the smallest molybdosiloxane ring that belongs to the di-oxo MoO_4 unit (Figure 3 a). Extending the 2D model into real 3D space further increases the number of combination possibilities available to silanol groups (even for the same size of molybdosiloxane ring).

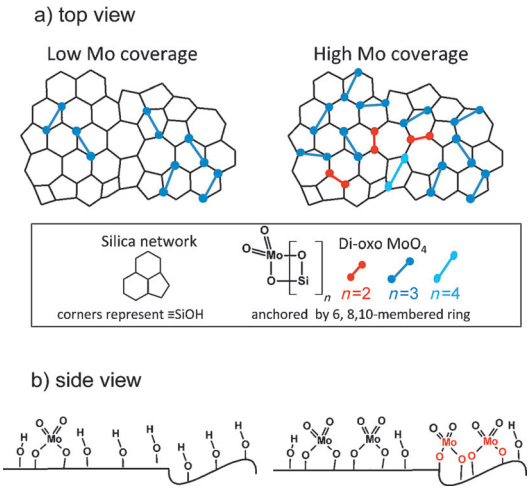

Figure 3. Proposed anchoring patterns of di-oxo (-Si-O-)$_2$Mo(=O)$_2$ structures on a 2D silica surface at different surface molybdenum densities. Two 2D models (a, b) are shown to illustrate the real 3D space. The colored dots linked by lines in the top view (a) represent the di-oxo species with different degrees of structural strain.

Strain at the anchoring bonds leads to a high potential energy at this location. Based on the Brønsted–Evans–Polanyi relation,[23,24] which seems applicable to metal oxides as well,[25] this increased potential energy enhances the reactivity. Accordingly, the increased reducibility at high Mo oxide coverage (Figure 1) is explained by the increased strain of parts of the surface where the Mo oxide species are predominantly di-oxo MoO_4 structures. The occurrence of a distinct low-temperature peak at 856 K in the H_2-TPR profile may reflect the presence of a discrete Si–Si distance (which may be related to a specific molybdosiloxane ring size) that accommodates a surface Mo oxide species that is particularly reactive towards hydrogen. This scenario is plausible because the flexibility of the siloxane network is not infinite.

As the occurrence of strain is closely related to the availability of anchoring surface hydroxy sites, tuning the silanol population by thermal treatment (i.e. variation in the dehydration temperature) instead of changing the metal loading would also allow the frustration to be controlled, leading to a change in the reactivity. In fact, the activity of silica-supported chromium oxide catalysts used in ethylene polymerization (Phillips catalysts) increases with increasing the activation temperature, up to 1198 K. The activation process causes a progressive dehydroxylation,[26–28] which may be rationalized in terms of an increased strain of the surface chromate species.[27–30]

To investigate the influence of the anchoring geometry on the O K-edge NEXAFS feature, we modeled a highly strained di-oxo (Si-O-)$_2$Mo(=O)$_2$ structure (cluster **c** in Figure S1) anchored on a silanol pair with a Si–Si distance of 3.07 Å, which is much shorter than that of other cluster models (4.6–4.7 Å; Figure S1, Table S1). The geometric constraint results in significant modification of the O=Mo=O angle and the Mo=O bond lengths, which drastically affects the NEXAFS feature (Table S1, Figure S5 A). Modification of the cluster model by changing the O=Mo=O bond angle while freezing the other geometric parameters results in a clear systematic change in the calculated O K-edge NEXAFS spectra. It was found that some of the angle-modified di-oxo clusters show intense absorption at 531 eV (Figure S5 B), which may account for the increased absorption at around 531 eV observed in the experimental spectra of the high-coverage samples (Figure 2 d). As MoO_x/SBA-15 consists of a distribution of species, as evidenced by H_2-TPR, the observed O K-edge NEXAFS spectra represent an integral of all the species present, which cannot be readily simulated by the limited number of model clusters considered herein. Nevertheless, these theoretical observations suggest that an increased distortion of the tetrahedral geometry of the (Si-O-)$_2$-Mo(=O)$_2$ units as a result of the limited space available on the silica surface may be the reason for the changes in the O K-edge NEXAFS spectra. The greater structure sensitivity of the O K-edge NEXAFS versus UV/Vis and Mo K-edge XANES data is because the O K-edge NEXAFS is based on the excitation of the electrons in the isotropic (i.e. spherical) O 1s core orbitals of all the O atoms coordinated to the Mo center into the unoccupied anisotropic Mo 4d–O 2p orbitals.

In addition to the strain imposed by the Mo–O–Si anchoring bonds, lateral interactions between vicinal surface Mo oxide species come into play at higher coverage, which can influence spectroscopic features and reactivity as well. The DFT calculations clearly reveal a repulsive interaction of two adjacent tetrahedral di-oxo MoO_4 units (cluster **b** in Figure S1). Increasing the surface density of MoO_x species may induce O–O interactions, resulting in a modification of the O = Mo = O angle or other geometric parameters. Likewise, structural perturbations as a result of the hydrogen

bonding between surface silanol groups and surface Mo oxide species may also influence the reactivity. In fact, the occurrence of hydrogen bonding is clearly visible in the O–H stretching region of the IR spectra (Figure S6C). The stretching vibrations arising from molybdenum–oxygen groups are shifted to lower wavenumbers in the Raman and IR spectra when the Mo oxide loading decreases and hydrogen bonding to neighboring silanol groups becomes more abundant (Figure S6B,D).

The H_2-TPR (Figure 1) probes the distribution of surface hydroxy species and provides information on all the hydroxy species present. Following Taylor's concept, it is expected that only a fraction of these site are "high-energy sites" that are reactive enough to perform catalytic turnovers in heterogeneously catalyzed reactions. Indeed, a steep increase in the catalytic activity at 8.2 % of Mo loading was observed in both propene metathesis and the oxidative dehydrogenation of propane (Figure 4), showing the significant impact resulting

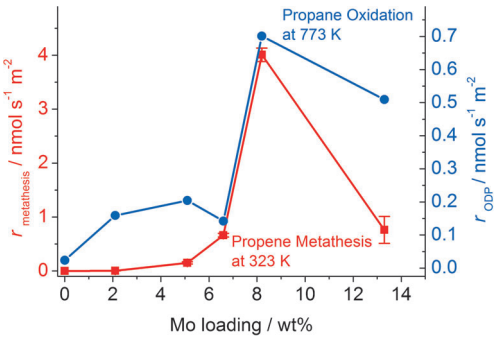

Figure 4. Specific rates of product formation for propene metathesis at 323 K (squares), and oxidative dehydrogenation of propane (ODP) at 773 K (circles) over MoO_x/SBA-15. Selectivity to desired product(s) was over 99.5 % and 49–83 % for propene metathesis and ODP, respectively. Selectivity data for ODP are presented in Figure S9.

from the strain of surface-anchored metal oxide species. Owing to the different reactants that have to be activated (H_2, propene, propane, and O_2) and, consequently, the different demands on the corresponding active sites (Figure 1, Figure 4, S9) the trends found for the three different, stoichiometric or catalytic, reactions are not the same. The most complex reaction within the series studied is the oxidative dehydrogenation of propane which involves a complex network of consecutive and parallel reactions that determine the selectivity (Figure S9). But also in that case the emerging strain of the surface metal oxide species with increasing loading is reflected in the formation rate of the product, because the activation of the methylene C–H bond in propane on surface metal oxide species has been shown to be the rate-determining step.[31]

In summary, the remarkable increase in the reactivity of silica supported molybdenum oxide species at high Mo oxide surface coverage is related to an increased frustration of the surface molybdenum oxide species, which originates from the geometric constraints of the anchoring bonds and additional lateral interactions of the surface species. Given the similarity in the molecular structures of supported metal oxides,[14] the same scenario is likely to occur in other monolayer-type supported metal oxides, especially for SiO_2 supports that tend to form isolated surface metal oxide sites.[14] Changing the support material (e.g. alumina, titania, zirconia) changes the nature of the supported metal oxide species win terms of both the distribution of suitable geometric arrangements[32] and the electronic properties.[33] Even given this complexity, strain-induced "high-energy sites," would occur locally at the metal oxide/support interface whenever a suitable distribution of anchoring sites exists, which is likely always the case.

We propose the frustration of the surface metal oxide species as an important and novel descriptor for catalysis over supported metal oxides to complement other structural classifications that have been considered (e.g. degree of polymerization, coordination patterns). Based on these insights, we argue that theoretical and experimental efforts in heterogeneous catalysis should focus more on metastable configurations that are usually less acknowledged because of their instability or minority status. Furthermore, applying the mechanistic concept for the formation of "high-energy sites" presented herein, a rational catalyst design would be feasible by choosing strategies that artificially increase the probability of the formation of "high-energy sites", for example, the use of promoter elements or tuning the surface structure of the support by physicochemical treatments (e.g. activation temperature as in the case of Phillips catalysts).

Experimental Section

The MoO_x/SBA-15 catalysts (Mo loading of 2.1–13.3 wt %/0.2–2.5 Mo-atoms nm^{-2}) were prepared by an ion-exchange approach. Details regarding synthesis, characterization, DFT calculations, and catalytic test reactions are summarized in the Supporting Information.

Received: July 29, 2013
Published online: November 20, 2013

Keywords: heterogeneous catalysis · molybdenum · olefin metathesis · oxidation · supported catalysts

[1] H. S. Taylor, *Proc. R. Soc. London Ser. A* **1925**, *108*, 105–111.
[2] T. Zambelli, J. Wintterlin, J. Trost, G. Ertl, *Science* **1996**, *273*, 1688–1690.
[3] M. Behrens, F. Studt, I. Kasatkin, S. Kuehl, M. Haevecker, F. Abild-Pedersen, S. Zander, F. Girgsdies, P. Kurr, B. L. Kniep, M. Tovar, R. W. Fischer, J. K. Norskov, R. Schloegl, *Science* **2012**, *336*, 893–897.
[4] I. X. Green, W. Tang, M. Neurock, J. T. Yates, *Science* **2011**, *333*, 736–739.
[5] K. Amakawa, S. Wrabetz, J. Kröhnert, G. Tzolova-Müller, R. Schlögl, A. Trunschke, *J. Am. Chem. Soc.* **2012**, *134*, 11462–11473.
[6] K. Chen, A. T. Bell, E. Iglesia, *J. Catal.* **2002**, *209*, 35–42.
[7] I. E. Wachs, *Catal. Today* **2005**, *100*, 79–94.
[8] T.-C. Liu, M. Forissier, G. Coudurier, J. C. Védrine, *J. Chem. Soc. Faraday Trans. 1* **1989**, *85*, 1607–1618.
[9] R. Thomas, J. A. Moulijn, *J. Mol. Catal.* **1982**, *15*, 157–172.
[10] Y. Lou, H. Wang, Q. Zhang, Y. Wang, *J. Catal.* **2007**, *247*, 245–255.

[11] M. Boer, A. J. Dillen, D. C. Koningsberger, J. W. Geus, M. A. Vuurman, I. E. Wachs, *Catal. Lett.* **1991**, *11*, 227 – 239.
[12] R. S. Weber, *J. Catal.* **1995**, *151*, 470 – 474.
[13] J. Handzlik, J. Ogonowski, *J. Phys. Chem. C* **2012**, *116*, 5571 – 5584.
[14] E. L. Lee, I. E. Wachs, *J. Phys. Chem. C* **2007**, *111*, 14410 – 14425.
[15] S. Chempath, Y. Zhang, A. T. Bell, *J. Phys. Chem. C* **2007**, *111*, 1291 – 1298.
[16] L. J. Gregoriades, J. Döbler, J. Sauer, *J. Phys. Chem. C* **2010**, *114*, 2967 – 2979.
[17] C. S. Guo, K. Hermann, M. Hävecker, J. P. Thielemann, P. Kube, L. J. Gregoriades, A. Trunschke, J. Sauer, R. Schlögl, *J. Phys. Chem. C* **2011**, *115*, 15449 – 15458.
[18] L. Lichtenstein, C. Büchner, B. Yang, S. Shaikhutdinov, M. Heyde, M. Sierka, R. Włodarczyk, J. Sauer, H.-J. Freund, *Angew. Chem.* **2012**, *124*, 416 – 420; *Angew. Chem. Int. Ed.* **2012**, *51*, 404 – 407.
[19] S. Bordiga, S. Bertarione, A. Damin, C. Prestipino, G. Spoto, C. Lamberti, A. Zecchina, *J. Mol. Catal. A* **2003**, *204 – 205*, 527 – 534.
[20] F. Tielens, C. Gervais, J. F. Lambert, F. Mauri, D. Costa, *Chem. Mater.* **2008**, *20*, 3336 – 3344.
[21] M. A. Banares, H. C. Hu, I. E. Wachs, *J. Catal.* **1994**, *150*, 407 – 420.
[22] S. Braun, L. G. Appel, V. L. Camorim, M. Schmal, *J. Phys. Chem. B* **2000**, *104*, 6584 – 6590.
[23] J. N. Bronsted, *Chem. Rev.* **1928**, *5*, 231 – 338.
[24] M. G. Evans, M. Polanyi, *Trans. Faraday Soc.* **1938**, *34*, 11 – 24.
[25] A. Vojvodic, F. Calle-Vallejo, W. Guo, S. Wang, A. Toftelund, F. Studt, J. I. Martinez, J. Shen, I. C. Man, J. Rossmeisl, T. Bligaard, J. K. Norskov, F. Abild-Pedersen, *J. Chem. Phys.* **2011**, *134*, 244509.
[26] B. M. Weckhuysen, I. E. Wachs, R. A. Schoonheydt, *Chem. Rev.* **1996**, *96*, 3327 – 3350.
[27] M. P. McDaniel, M. B. Welch, *J. Catal.* **1983**, *82*, 98 – 109.
[28] M. P. McDaniel in *Handbook of Heterogeneous Catalysis*, Wiley-VCH, Weinheim, **2008**.
[29] E. Groppo, C. Lamberti, S. Bordiga, G. Spoto, A. Zecchina, *Chem. Rev.* **2005**, *105*, 115 – 184.
[30] C. A. Demmelmaier, R. E. White, J. A. van Bokhoven, S. L. Scott, *J. Catal.* **2009**, *262*, 44 – 56.
[31] X. Rozanska, R. Fortrie, J. Sauer, *J. Phys. Chem. C* **2007**, *111*, 6041 – 6050.
[32] G. Tsilomelekis, S. Boghosian, *Catal. Sci. Technol.* **2013**, *3*, 1869 – 1888.
[33] T. Fievez, P. Geerlings, B. M. Weckhuysen, F. De Proft, *ChemPhysChem* **2011**, *12*, 3281 – 3290.

